

An entirely reverse-engineered finite element model of a classical guitar in comparison with experimental data

Alexander Brauchler, Pascal Ziegler and Peter Eberhard

Citation: *The Journal of the Acoustical Society of America* **149**, 4450 (2021); doi: 10.1121/10.0005310

View online: <https://doi.org/10.1121/10.0005310>

View Table of Contents: <https://asa.scitation.org/toc/jas/149/6>

Published by the *Acoustical Society of America*

ARTICLES YOU MAY BE INTERESTED IN

[Acoustic characterisation of string instruments by internal cavity measurements](#)

The Journal of the Acoustical Society of America **150**, 1922 (2021); <https://doi.org/10.1121/10.0006205>

[Eigenfrequency optimisation of free violin plates](#)

The Journal of the Acoustical Society of America **149**, 1400 (2021); <https://doi.org/10.1121/10.0003599>

[Exploring design variations of the Titian Stradivari violin using a finite element model](#)

The Journal of the Acoustical Society of America **148**, 1496 (2020); <https://doi.org/10.1121/10.0001952>

[Electric-to-acoustic pickup processing for string instruments: An experimental study of the guitar with a hexaphonic pickup](#)

The Journal of the Acoustical Society of America **150**, 385 (2021); <https://doi.org/10.1121/10.0005540>

[State-space modeling of sound source directivity: An experimental study of the violin and the clarinet](#)

The Journal of the Acoustical Society of America **149**, 2768 (2021); <https://doi.org/10.1121/10.0004241>

[Spectral envelope position and shape in sustained musical instrument sounds](#)

The Journal of the Acoustical Society of America **149**, 3715 (2021); <https://doi.org/10.1121/10.0005088>

JASA
THE JOURNAL OF THE
ACOUSTICAL SOCIETY OF AMERICA

CALL FOR PAPERS

**Special Issue: Fish Bioacoustics:
Hearing and Sound Communication**

An entirely reverse-engineered finite element model of a classical guitar in comparison with experimental data^{a)}

Alexander Brauchler,^{b)} Pascal Ziegler, and Peter Eberhard^{c)}

Institute of Engineering and Computational Mechanics, University of Stuttgart, Pfaffenwaldring 9, Stuttgart, 70569, Germany

ABSTRACT:

The classical guitar is a popular string instrument in which the sound results from a coupled mechanical process. The oscillation of the plucked strings is transferred through the bridge to the body, which acts as an amplifier to radiate the sound. In this contribution, a procedure to create a numerical finite element (FE) model of a classical guitar with the help of experimental data is presented. The geometry of the guitar is reverse-engineered from computed tomography scans to a very high level of detail, and care is taken in including all necessary physical influences. All of the five different types of wood used in the guitar are modeled with their corresponding orthotropic material characteristics, and the fluid-structure interaction between the guitar body and the enclosed air is taken into account by discretizing the air volume inside the guitar with FEs in addition to the discretization of the structural parts. Besides the numerical model, an experimental setup is proposed to identify the modal parameters of a guitar. The procedure concludes with determining reasonable material properties for the numerical model using experimental data. The quality of the resulting model is demonstrated by comparing the numerically calculated and experimentally identified modal parameters. © 2021 Acoustical Society of America. <https://doi.org/10.1121/10.0005310>

(Received 28 January 2021; revised 21 May 2021; accepted 27 May 2021; published online 24 June 2021)

[Editor: Vasileios Chatziioannou]

Pages: 4450–4462

I. INTRODUCTION

The human fascination with music and musical instruments is as old as humankind itself. Some instruments, like the violins made by Stradivari or the guitars made by Torres, have delighted musicians and audiences for centuries. Many among them are still of the opinion that the sound of these instruments is unmatched by the work of contemporary luthiers, albeit recent studies reported that even trained musicians did not necessarily choose old master instruments over new ones (Fritz *et al.*, 2012; Saitis *et al.*, 2012). Nevertheless, musicians are able to distinguish between instruments by the subtle differences and, thus, even seemingly equal instruments differ in their sounds. In science, an increasing number of numerical models are used with the aim to enhance the understanding of the physical processes in the instruments and explain these subtle differences between the instruments. One popular string instrument is the classical guitar, in which the sound results from a coupled mechanical process. The oscillation of the plucked strings is transferred through the bridge to the guitar body, which interacts with the enclosed and surrounding air to radiate the tone of the instrument.

Numerical modeling of string instruments and, specifically, guitars emerged several decades ago with the modeling of the strings. Beginning with the one-dimensional wave equation to simulate the oscillation of an isolated string (see

Hiller and Ruiz, 1971), models have been extended by bending the stiffness to incorporate the effect of dispersion, and sophisticated damping models have been developed (Ducceschi and Bilbao, 2016; Woodhouse, 2004a,b). Recent string models, in good agreement with the measurements, are even able to predict contact between a string and the frets of an electric bass or simulate the coupling between the different polarizations of the transversal string oscillation (Brauchler *et al.*, 2020a; Issanchou *et al.*, 2018).

In parallel, numerical models for the instrument's body have been developed. Different modeling approaches, like finite difference models (Bader, 2006), models using spectral methods (Derveaux *et al.*, 2003), or multibody models (Caldersmith, 1978; Christensen, 1982; French, 2007; Popp, 2012), have been evaluated. The most applied method is, however, the finite element (FE) method, which, in the beginning, has been used to examine the influence of the soundboard's thickness (Richardson and Roberts, 1983). Further studies modeled and analyzed the guitar soundboards in different states during the production process (Elejabarrieta *et al.*, 2000), and the influence of the fluid-structure interaction between the guitar body and enclosed air has been quantified (Ezcurra *et al.*, 2005). Exploiting symmetries in the model can make the simulation procedure more efficient and even the sound radiation is calculated (Bécache *et al.*, 2005; Stanciu *et al.*, 2019). Besides that, FE models are used for sound synthesis and to support the design process of the instruments (Torres and Boullosa, 2009; Torres *et al.*, 2020; Välimäki *et al.*, 2006). Current models assist the conservation of old instruments with high cultural value (Konopka *et al.*, 2017; Viala *et al.*, 2020) and

^{a)}This paper is part of a special issue on Modeling of Musical Instruments.

^{b)}Electronic mail: alexander.brauchler@itm.uni-stuttgart.de, ORCID: 0000-0002-2359-4206.

^{c)}ORCID: 0000-0003-1809-4407.

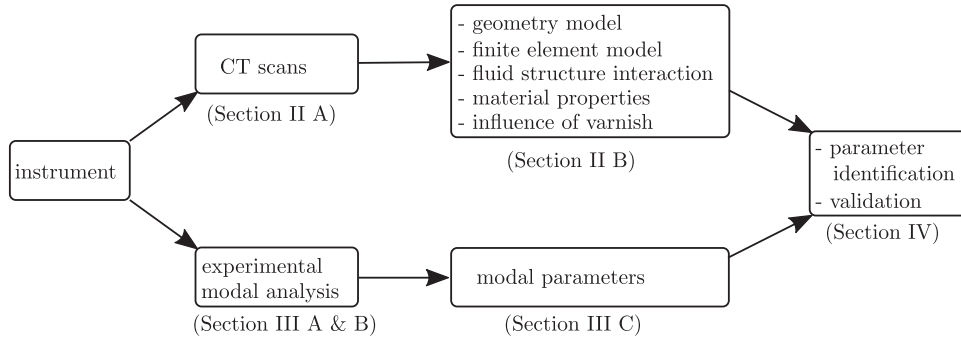


FIG. 1. Flow chart of the proposed reverse-engineering procedure.

due to good agreement with the measurements, can be used as virtual prototypes (Tahvanainen *et al.*, 2019).

To validate these numerical models, generally, transfer functions and modal parameters, such as eigenfrequencies and mode shapes, are compared with experimentally identified ones (Brauchler *et al.*, 2020b; Tahvanainen *et al.*, 2019). The modal parameters of a structure can be identified via experimental modal analyses (Ewins, 2000). In a modal analysis, the structure is normally excited by an impulse hammer or electrodynamical shaker and the input force, as well as the oscillation of the structure, is measured usually by force sensors and accelerometers. Particularly interesting for sensitive musical instruments are the completely contactless excitation and measurement methods and operational modal analyses. An instrument can be excited by a loudspeaker or simply by plucking its strings, and the velocity on the surface may be measured by a laser Doppler vibrometer (LDV) as was previously done for the isolated instrument parts or a complete concert harp (Chomette and Le Carrou, 2015; Viala *et al.*, 2018). Moreover, experimental approaches are applied to develop methods to evaluate the quality of the instruments and influence of the different types of wood (Boullosa, 2002; Šali and Kopač, 2000; Torres and Torres-Martínez, 2015).

Although there are all of these research efforts, some details of the old master instruments still remain uncharted. With the growing computational power, it might now be possible to identify unknown parameters of such old, valuable instruments while being completely nondestructive. The research question the authors propose is, consequently, to create a numerical model of a classical guitar with such a high level of detail that it will be possible to noninvasively identify unknown material parameters of an existing instrument.

In this contribution, a procedure is presented to create a geometrically and physically highly detailed FE model of an existing instrument using computed tomography (CT) without harming the instrument in any way. The model contains multiple orthotropic materials and takes the fluid-structure interaction between the guitar body and enclosed air into account. Furthermore, an experimental setup is developed and an experimental modal analysis is conducted, resulting in reliably identified modal parameters of the existing instrument. Finally, the modal parameters of the numerical model

and the parameters identified with the experimental modal analysis are compared, and a parameter identification procedure is proposed to determine the unknown material properties of the instrument under investigation. The model might be used to gain further insight into already existing, possibly very old, and expensive instruments. Although other researchers used CT scans to model the musical instruments, e.g., Pyrkosz (2013), to the authors' knowledge, a completely reengineered model for a classical guitar to the presented level of detail does not yet exist. The suggested procedure to reverse-engineer a FE model from an existing instrument might guide further researchers to create detailed numerical models of string instruments and is briefly represented in Fig. 1.

II. REVERSE-ENGINEERING A VIRTUAL GUITAR

The instrument under investigation is a decent, mid-priced classical guitar of type Yamaha GC-12 (Hamamatsu, Japan). It is made completely of solid wood with a cedar top and mahogany back and sides, and the applied bracing pattern is a slightly unsymmetric Torres bracing as can be seen in Fig. 2. In the following, the modeling procedure with the help of CT scans and the attributes of the numerical model, including multiple orthotropic materials and the fluid-structure interaction, are described. The FE modeling and

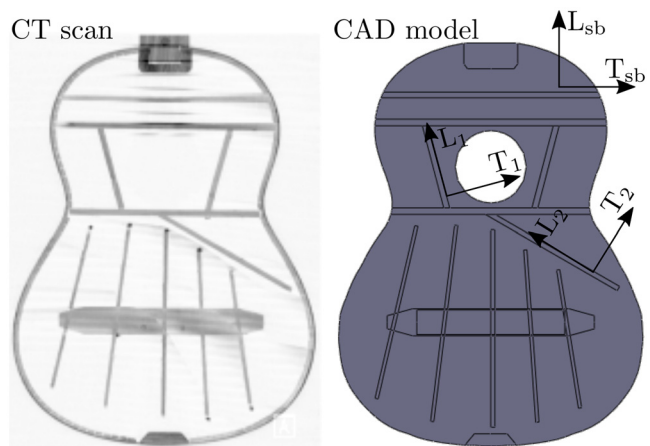


FIG. 2. (Color online) Comparison between the CT scan (left) and geometry model (right) of the guitar soundboard's bracing pattern. The material coordinate systems are included for the soundboard and two struts as an example.

simulations are performed with the commercial software ABAQUS, and for details on the FE backgrounds, the reader is referred to the ABAQUS reference (Abaqus, 2014).

A. Geometry modeling

Modeling the geometry of an existing guitar can be an elaborate task. Although measuring the geometry of the parts that are visible from the outside is straightforward, it is difficult to measure the details of the bracing pattern inside the guitar body by hand through the soundhole. Unlike many technical systems, a guitar cannot simply be disassembled to measure the position and shape of the parts inside without expecting a different behavior after gluing the parts back together. To avoid harming the instrument by disassembling or erroneous measurements by gauging through the soundhole, the CT scans of the guitar body have been made in cooperation with the Department of Diagnostic and Interventional Radiology of the *Klinikum Stuttgart* (Germany). Briefly, CT is an imaging technique that makes use of multiple x-ray measurements taken from different angles, either by rotating the x-ray source (as has been done here) or the specimen to be measured to generate cross-sectional images of the specimen (Buzug, 2011). With this procedure, cross-sectional images of the guitar body in all three dimensions have been generated with a distance of 0.6 mm in between each image and a resolution of approximately 0.5 mm. In total, around 2000 images have been evaluated and used to take measurements to create the geometric model of the guitar.

One such image representing a cross section that is parallel to the top of the guitar directly beneath the soundboard is displayed in Fig. 2. From this image, it is possible to extract the bracing pattern as well as the width of the 11 struts on the soundboard and other visible parts like the support of the bridge and connection with the neck. The bracing pattern on the soundboard and back of the guitar have a crucial influence on the oscillation behavior and, hence, on the sound of the instrument. On the one hand, the bracing is necessary to reinforce the soundboard to withstand the forces exerted by the strings, and on the other hand, it is a design parameter for luthiers to influence the eigenfrequencies and mode shapes of the instrument. The extracted pattern of the soundboard used for the FE model is shown on the right-hand side of Fig. 2. The largest difference between the two images remains the soundhole, which is not visible in this cross-sectional image from the CT, which was taken beneath the soundhole.

As all of the struts are unique in their size and shape, they need to be modeled one by one using cross-sectional images. In Fig. 3, as an example, the cross-sectional images used to model the middle strut on the back of the guitar can be compared to the resulting model of the part. Although it is visible that the resolution of the images is not perfect when looking at the cross section of the strut, the resulting geometry for the FE model is still satisfyingly similar. Additionally, it is possible to distinguish between the

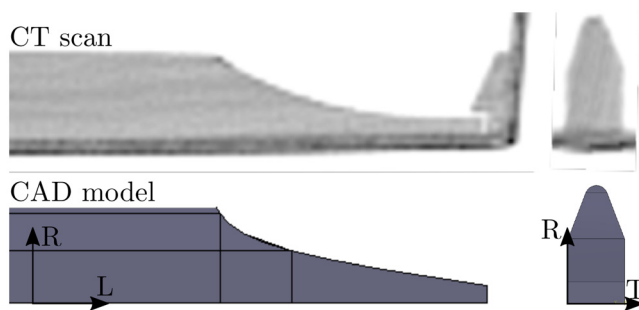


FIG. 3. (Color online) The CT scan cross-sectional image of the middle strut on the back of the guitar (top) and corresponding geometric model (bottom).

different types of wood and, hence, between the parts. The mahogany of the guitar's back plate is denser and, therefore, in the image, it is darker than the spruce of the strut. Even the grain direction of the wood can be identified from the images. This is crucial and results from the orthotropic material behavior of the wood.

Figure 4 depicts a cut through the resulting model of the guitar, consisting of 36 different parts, where the high level of detail is visible. The geometric modeling procedure is performed in ABAQUS with the necessity in mind that all parts need to be meshable. Consequently, no further adjustments on the parts geometries need to be made for the FE model.

B. FE model

In the FE model, the 36 different parts are meshed individually and then bound together via tie-constraints. These tie-constraints bind the movement of the slave nodes rigidly to those of their adjacent master nodes. Although this is an idealization of the glued connections between the parts, it is expected to yield reasonably good results (Tahvanainen et al., 2019). The model contains shell elements whenever applicable, leading to linear shell elements of ABAQUS type S4 for the discretization of the soundboard, back, and sides of the guitar. All other parts are discretized with the linear volume elements of ABAQUS type C3D8 as indicated in Fig. 4.

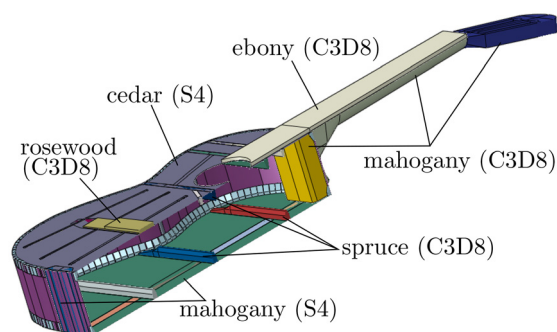


FIG. 4. (Color online) The cut through the resulting geometry of the FE model.

In addition, the five different wooden materials of the distinct guitar parts are labeled. Whereas the majority of parts, namely, the back, sides, neck, and headstock, are made out of mahogany, the soundboard of the guitar is comprised of cedar. Additional parts are the ebony fretboard, rosewood bridge, and struts and linings, which are made out of spruce. Not yet included in the model are the strings and machine heads of the guitar as the focus is set on the behavior of the guitar body without any geometric stiffness effect caused by the string forces exerted on the guitar. Hence, the strings and machine heads are also dismantled during the experimental studies.

The elastic material behavior of wood can be characterized as orthotropic. So, to describe the elastic behavior of each wood type, three Young's moduli E_L , E_T , and E_R , three shear moduli G_{LT} , G_{LR} , and G_{TR} , and three Poisson ratios ν_{LT} , ν_{LR} , and ν_{TR} need to be defined depending on the grain direction and growth rings of the wood. The longitudinal direction (index L) is defined along the fiber direction, and the tangential (index T) and radial (index R) directions are perpendicular to this depending, additionally, on the growth rings (Kretschmann, 2010). This is an appropriate and useful model, albeit material testing reveals that the elastic behavior of wood is even more complex, yielding a nonsymmetric compliance matrix in reality (Kretschmann, 2010). The elastic material properties used in the FE model are summarized in Table I. Due to a lack of data, the material properties perpendicular to the fiber direction in ebony and rosewood are approximated to behave in a way that is similar to the other wood types.

One mostly neglected but influential aspect is the varnish on the guitar, which is known to influence the longitudinal and radial material properties as well as increase the mass of the guitar through areal mass loading on the coated parts (Lämmlein et al., 2020). Usually, the elastic properties of wood tend to be linearly related to its density (Wegst, 2006). However, owing to the largely deviating influences of the different varnish types and unknown type of varnish on the examined instrument, the influence of the varnish on the stiffness of the materials has to be neglected. On the other hand, the mass increase, at least, can be approximated by comparing the weight of the real instrument to the weight calculated for its virtual counterpart. Weighing the instrument under investigation without machine heads yields a mass of $m_G = 1432$ g, the calculation of the mass of the FE model, however, results in only $m_{FE} = 1230$ g. Because the geometry of the model should be quite similar to that of the

real instrument, it is now assumed that the mass difference has to be the result of the missing mass of the varnish and erroneous density values from the literature, where the wood density is known to vary significantly between different specimens and different moisture content and can be calculated as

$$m_G - m_{FE} = m_{\text{varn}} + \sum \Delta\rho_k V_k, \tag{1}$$

where the mass of the varnish is m_{varn} , the deviation of the densities for the different sorts of wood is $\Delta\rho_k$, and the corresponding volumes are V_k . If it is now further supposed that the varnish has a typical density of $\rho_{\text{varn}} = 1.2$ kg/m³ and is only applied on the soundboard (area, $A_{\text{sb}} = 0.14$ m²), the back ($A_b = A_{\text{sb}}$), and the sides ($A_s = 0.134$ m²) in a layer with thickness $d = 0.3$ mm, the total weight of the varnish will sum up to $m_{\text{varn}} = 149$ g. The resulting areal mass loading of 360 g/m² is quite high, but according to values from the literature, it is still in a realistic range (Lämmlein et al., 2020). This additional mass of the varnish is applied to the FE model in a simplified manner by modifying the density of the soundboard to $\rho_{\text{cedar}} = 420$ kg/m³ and the density of the back and sides to $\rho_{\text{mahag}} = 540$ kg/m³. The total mass of the guitar model, including the increased mass due to the varnish, is $m_{\text{vFE}} = 1380$ g and, thus, fairly similar to the mass of the real guitar.

Another very typical and highly influential physical effect within guitars is the fluid-structure interaction between the guitar body and enclosed air. Whereas in many technical systems, the coupling of a vibrating structure with the air can be described as a weak coupling, meaning an essentially unilateral influence of the structure on the air, and guitars yield a special case. The air cavity inside the guitar with the opening of the soundhole can be characterized as a Helmholtz resonator having its first resonance frequency very close to the first out-of-plane mode, often referred to as the (0,0)-mode, of the guitar body (Fletcher and Rossing, 1991). In combination with the thin and light wooden plates constituting the guitar body, this leads to a strong coupling between the structural guitar body and enclosed air, which must not be neglected in any serious guitar model.

The air cavity is included in the FE model by discretizing the cavity inside the guitar with linear, pressure-based acoustic elements of ABAQUS type AC3D8. The complete system of equations for the dynamics of the undamped system with acoustic structural coupling is of the form

TABLE I. Material parameters for the different materials of the guitar model taken from Kretschmann (2010) and Gore (2011).

Material	ρ (kg/m ³)	E_L (GPa)	E_T (GPa)	E_R (GPa)	G_{LT} (GPa)(GPa)	G_{LR} (GPa)	G_{TR} (GPa)	ν_{LT}	ν_{LR}	ν_{TR}
Mahogany	420	10.7	0.534	1.18	0.630	0.939	0.224	0.641	0.297	0.264
Cedar	320	8.47	0.466	0.686	0.728	0.737	0.042	0.296	0.378	0.403
Spruce	400	11.9	0.511	0.927	0.725	0.760	0.036	0.467	0.372	0.245
Ebony	1100	17.6	0.880	1.76	1.23	1.58	0.352	0.3	0.35	0.35
Rosewood	775	13.5	0.700	1.40	1.00	1.30	0.30	0.3	0.35	0.35

$$\begin{bmatrix} \mathbf{M}_F & \rho_F \mathbf{C}^T \\ 0 & \mathbf{M}_S \end{bmatrix} \begin{bmatrix} \ddot{\mathbf{p}} \\ \ddot{\mathbf{u}} \end{bmatrix} + \begin{bmatrix} \mathbf{K}_F & 0 \\ -\mathbf{C} & \mathbf{K}_S \end{bmatrix} \begin{bmatrix} \mathbf{p} \\ \mathbf{u} \end{bmatrix} = \mathbf{0}, \quad (2)$$

containing the mass matrices of the fluid \mathbf{M}_F and structure \mathbf{M}_S , stiffness matrices of the fluid \mathbf{K}_F and structure \mathbf{K}_S , coupling matrix \mathbf{C} , and the pressure and displacement degrees of freedom \mathbf{p} and \mathbf{u} . To characterize the air, values at 20 °C are applied, namely, the density $\rho_F = 1.2 \text{ kg/m}^3$ and speed of sound $c = 343 \text{ m/s}$. The calculation of the coupling term follows from a nodewise application of

$$\frac{\partial p}{\partial n} = -\rho_F \frac{\partial^2}{\partial t^2} u_n, \quad (3)$$

where n defines the normal direction and either the pressure p is specified or the displacement in the normal direction u_n of the boundary is prescribed, depending on which side of the coupling is considered. In addition, on the free boundary of the soundhole, acoustic infinite elements of ABAQUS ACIN3D4 are applied to simulate a radiation condition into an infinite domain, the details of which can be found, for example, in [Abaqus \(2014\)](#) and [Sigrist \(2015\)](#). In total, the degrees of freedom in the model sum up to 571 671.

To highlight the effect of the acoustic structural coupling on the model behavior, the eigenfrequencies of the fully coupled model are compared with those of the two uncoupled systems. Therefore, in Fig. 5, the eigenfrequencies of the coupled model, the uncoupled air model, and the uncoupled structural model are depicted. Although the air model has only one resonance in the displayed frequency range up to 270 Hz, the Helmholtz resonance frequency, the uncoupled structural model, has five eigenfrequencies in that range. In the following, the coupling between the Helmholtz resonance of the air and first structural modes is interpreted. Nevertheless, the air model produces higher order modes as well, which couple to higher order modes of the structure. A strong influence of the coupling is clearly visible when comparing the eigenfrequencies of the coupled

model to the other two models. Three of the five visible eigenfrequencies are significantly different and a sixth eigenfrequency is apparent. The coupling effect is even more vivid when looking at the relative change of eigenfrequencies of the most similar modes between the uncoupled and coupled structural models. The eigenfrequencies of mode 1 and mode 3, the in-phase and out-of-phase (0,0)-modes, respectively, decrease by more than 20% through the physically required coupling. This strong effect on the eigenfrequencies can be explained by the similar frequencies of the Helmholtz mode of the air at 133 Hz and the (0,0)-mode of the uncoupled structure at 137 Hz. Mode 2, the first bending mode, and mode 4, the twisting mode, on the other hand, are only slightly affected with a relative frequency change below 5%. This is exactly what would be the expected effect of the fluid-structure interaction as the modes where fluid and structure are strongly interacting show a large frequency change while the frequencies of the modes with a low interaction of fluid and structure barely change at all.

To sum up this section, a FE model of a classical guitar has been created from CT scan images to a very high level of detail. The five different kinds of woods are included in the model with their orthotropic material properties and the additional weight of the varnish is taken into account. Furthermore, the model contains the fluid-structure interaction between the guitar body and enclosed air, yielding an influence in the model as expected in theory.

III. EXPERIMENTAL MODAL ANALYSIS

An experimental modal analysis of the guitar is performed to serve as a reference solution against which the FE model can be validated and compared. Comparing the modal parameters, especially the eigenfrequencies and mode shapes, is a reliable way to assess the similarity between the model and reality. Additionally, the modal damping ratios are identified, which are necessary to simulate the transfer functions and transients with the numerical model realistically. They also help to gain further insight into the specific instrument’s vibrational behavior. First, the experimental setup and method used for the modal analysis are described. Then, for the analysis, a method using the complex mode indicator function (CMIF) and enhanced frequency response functions (EFRFs) is used ([Allemang and Brown, 2006](#)). This is followed by a summary of the experimental results.

A. Experimental setup

The experimental setup shown in Fig. 6 consists of the guitar hanging on springs from an aluminum frame as well as an automatic impulse hammer and a scanning LDV. The soft springs suspending the guitar are attached at the position of the nut to realize approximately free boundary conditions. Due to their significant weight of 160 g, the machine heads were removed before the measurements to obtain results comparable to the FE model. The design of the setup

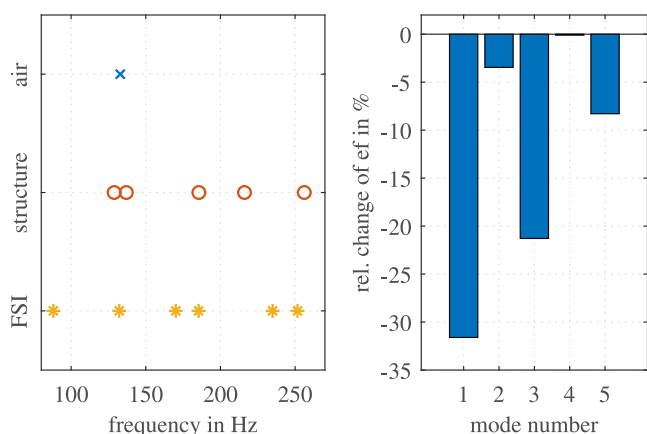


FIG. 5. (Color online) (Left) The first eigenfrequencies of the air cavity with rigid boundaries, the structural model without air, and the model with acoustic structural coupling. (Right) The relative change of eigenfrequencies of the model with an acoustic structural coupling compared to the structure only model.

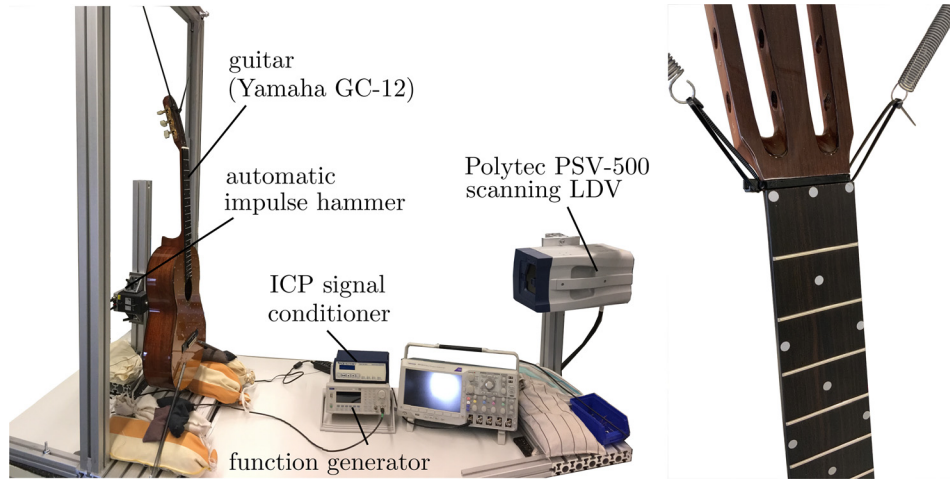


FIG. 6. (Color online) The experimental setup for the modal analysis (left) and close-up of the suspension on the nut of the guitar (right).

makes it easily possible to turn the guitar around and thereby measure the vibration on the front as well as on the back of the guitar. This is an alternative to the application of mirrors to measure the velocity on points around the complete guitar with a LDV. The velocity at these predefined points on the guitar is measured with a Polytec PSV-500 scanning LDV (Waldbronn, Germany), which allows for the completely noninvasive measurement of the different points on the guitar without moving the LDV.

The excitation of the guitar is realized via a modified electrodynamical shaker that acts like an automatic impulse hammer. During the measurement, the shaker is triggered by a function generator with a short trigger signal, which leads to a single hammering motion of the shaker. A soft rubber tip is used to avoid possible damage to the guitar under test, and the contact force is measured by an integrated circuit piezoelectric (ICP) sensor. The shaker can be moved around the guitar to accomplish multiple excitation positions.

B. Parameter identification method

With all of their advantages and disadvantages, a plethora of methods to identify the modal parameters of a system through experimental modal analysis exists. The presented experimental setup with the scanning LDV allows for measurements at many different points. Due to its advantage of making use of this fine spatial resolution of the measurements, the CMIF, in combination with EFRFs, is used for the modal analysis. In the following, the combined method shall be briefly explained while a thorough description of the method can be found in [Allemang and Brown \(2006\)](#).

It is supposed that the force input $f_k(t)$ and velocity output $v_j(t)$ are measured at multiple positions and their Fourier transforms are $F_k(\omega)$ and $V_j(\omega)$. The input positions are denoted $k = 1, 2, \dots, K$ and the output positions are denoted $j = 1, 2, \dots, J$. Accordingly, the matrix of mobilities $Y(\omega)$, which is a complex $J \times K$ matrix, is used to provide a basis for the parameter identification with the modal analysis and can be calculated in a piecewise manner from

$$Y_{jk}(\omega) = \frac{V_j(\omega)}{F_k(\omega)}. \tag{4}$$

From the real part of $Y(\omega)$, the CMIF is calculated through a singular value decomposition at each considered frequency, which results in

$$\text{Re}(Y(\omega)) = U(\omega)\Sigma(\omega)V(\omega)^H, \tag{5}$$

where $U(\omega)$ is the real $J \times J$ matrix of left singular vectors, $V(\omega)$ is the real $K \times K$ matrix of right singular vectors, and $\Sigma(\omega)$ is the real $J \times K$ matrix of singular values. The superscript “H” denotes the Hermitian of a matrix. For each reference (input position) k , one singular value can be calculated, and these singular values at the considered frequencies, then, form the CMIF

$$\text{CMIF}_k(\omega) = \Sigma_k(\omega) \text{ with } k = 1, 2, \dots, K. \tag{6}$$

The resulting CMIF contains peaks for all of the modes existing in the data and forms a vector with K entries at each discrete frequency. It is advantageous over single mobilities as, in contrast to a single mobility, all eigenfrequencies occur as peaks in the CMIF, and even peaks very close to each other in the frequency range can be reliably identified. Consequently, frequencies at which peaks occur are used to identify the modal parameters of the system.

After identifying the eigenfrequencies ω_r in the CMIF, the left singular vectors $u_r(\omega_r)$ of dimension $J \times 1$ and the right singular vectors $v_r(\omega_r)$ of dimension $K \times 1$ at these eigenfrequencies are used to transform the matrix of mobilities into the modal domain and form a scalar EFRF,

$$\bar{Y}_r(\omega) = u_r^T Y(\omega) v_r, \tag{7}$$

for each mode. Note that the left singular vectors $u_r(\omega_r)$ are often already quite good approximations for the mode shapes of the system. If a sufficient spatial resolution of measurements is ensured, the EFRFs will form a curve for each mode without any influence of the neighboring modes.

Then, standard single degree of freedom parameter identification techniques are applicable to identify the modal parameters with high precision for each mode separately with the corresponding EFRF. In the presented case, a least squares peak fitting method is applied on the EFRFs to identify the modal parameters (Ewins, 2000).

With the identified modal parameters, it is then possible to reconstruct the EFRFs as separate single degree of freedom systems,

$$\bar{Y}_{rec}(\omega) = \frac{{}_r\bar{A}}{\omega_r^2 - \omega^2 + 2i\omega_r\omega\zeta_r}, \quad (8)$$

where ${}_r\bar{A}$ are the modal constants of the EFRFs and ζ_r are the modal damping coefficients. Then, these reconstructed EFRFs are transformed back into the physical domain and summed up to form the reconstructed matrix of mobilities,

$$Y_{rec}(\omega) = \sum_{r=1}^R \mathbf{u}_r \bar{Y}_{rec}(\omega) \mathbf{v}_r^T, \quad (9)$$

where R is the total number of identified modes in the considered frequency range and $Y_{rec}(\omega)$ is of the same size as $Y(\omega)$. To process all of the discrete frequencies, these matrices are stored as three-dimensional arrays of size $J \times K \times N_{freq}$, in practice, where N_{freq} denotes the total number of discrete frequencies.

C. Modal analysis results

For the experimental modal analysis, a total of 452 mobilities were measured. These measurements are composed of 133 points on the soundboard and fretboard and 93 points on the back of the guitar, where the velocity is measured with the LDV, resulting in the number of output positions $J = 226$. Moreover, the number of excitation positions is $K = 2$, consisting of one input position on the bottom right corner of the soundboard and one on the bottom right corner of the back. Each measurement takes as long as $T = 0.8$ s with a time resolution of $\Delta t = 8 \times 10^{-5}$ s, resulting in a frequency resolution of $\Delta f = 1.25$ Hz and a number of discrete frequencies $N_{freq} = 5000$ for their Fourier transforms. Longer measurements would result in zero-padding due to the faded signal and are, therefore, avoided. The matrix of mobilities for all discrete frequencies calculates to a three-dimensional array with size $226 \times 2 \times 5000$. The measurement mesh is depicted in Fig. 15, and the excitation is visible in terms of the positions where the measurement data is missing due to the shadow of the shaker.

To evaluate up to which frequency range a parameter identification is meaningfully possible, the input force signal is consulted. In Fig. 7, the force signal for ten consecutive measurements is displayed in the time and frequency domain. First and foremost, the signal is well shaped without any double hits, and the time in contact is about 1 ms. The signal yields a very good reproducibility, and the force is always below 2.5 N and, thus, sufficiently small to ensure

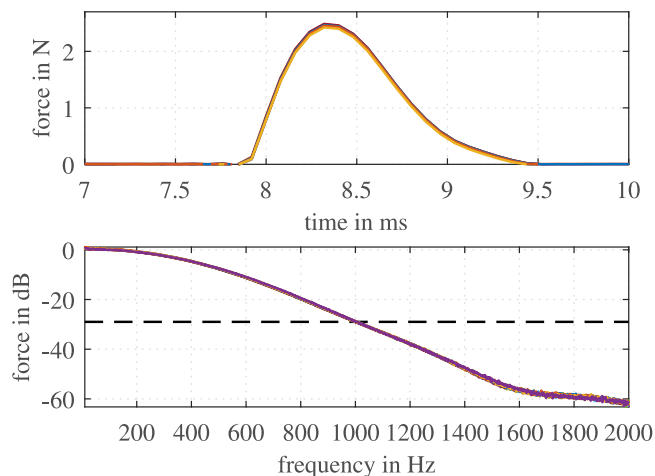


FIG. 7. (Color online) Ten consecutive hammer impact signals in the time domain (top) and frequency domain (bottom).

that the instrument is not harmed by the impulses. From the curves in the frequency range, it can be further concluded that frequencies up to 800 Hz are excited well as the signal is always above -20 dB up to that frequency. The parameter identification is even performed up to 1000 Hz as the LDV is known to yield a very good signal-to-noise ratio and the force signal at 1000 Hz is still slightly above -30 dB.

Figure 8 shows the CMIF calculated from the matrix of mobilities in a frequency range up to 1000 Hz with the identified eigenfrequencies highlighted. Two curves are displayed, one being the first singular value at each frequency point and the other is the second singular value at each frequency point because two references are used. In the evaluated frequency range, 41 eigenfrequencies are found. Most of them are found in the first CMIF, and the density of eigenfrequencies increases for higher frequencies as is expected for guitars. At each of the highlighted eigenfrequencies, an EFRF is calculated and the parameter identification is performed on these EFRFs. Furthermore, as several peaks occur very close to each other in the frequency range, e.g., the first two, the advantages of the CMIF/EFRF method

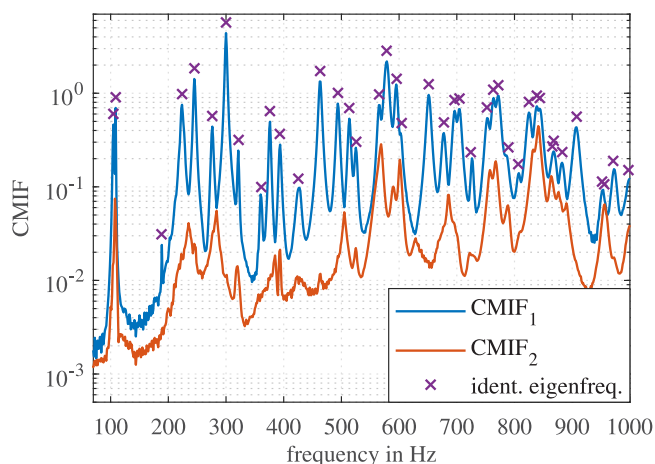


FIG. 8. (Color online) The CMIF with identified eigenfrequency locations.

may be emphasized here. Due to the projection with the singular vectors, these close peaks can be identified without the influence of their neighbors as long as the spatial resolution of measurements is fine enough. Hence, a very reliable and transparent parameter identification for these close eigenmodes is yielded. For the sake of brevity, only the final results of that procedure are presented hereafter.

An appraisal of the modal analysis results and, therefore, the quality of the identified modal parameters is possible in a straightforward manner by comparing the measured mobilities with the mobilities reconstructed from the identified modal parameters. Consequently, the measured and reconstructed mobilities are confronted in Figs. 9 and 10 in magnitude and phase, respectively, for two different input output combinations. Figure 9 shows the mobility with the input on the front and output on the soundboard closely below the bridge, whereas in Fig. 10, the mobility with the excitation on the back and velocity measurement on the upper middle part of the back is displayed. Two general conclusions can be drawn up front. First, the quality of the measurements is well suited for the parameter identification up to 1000 Hz because even close to 1000 Hz, no significant noise is visible, and the frequency resolution is clearly sufficient. Second, the reconstructed mobilities approximate the measurements remarkably well in magnitude and phase, indicating a successful parameter identification. The only clear deviation between the reconstruction and measurement is visible in Fig. 10 between 700 and 800 Hz, where the reconstructed phase is erroneous and the damping ratio of two eigenfrequencies seems to be too high, according to the width of the peaks. All in all, the identified modal parameters should be well suited as the reference solution for the numerical model.

Additionally, the mobility in Fig. 9, especially, allows for some interpretations about the instrument as the output position below the bridge is where large parts of the sound are radiated. Even better would be measurements with excitation on the bridge, but these would spoil the identified mode shapes as a result of the shadow of the shaker. The

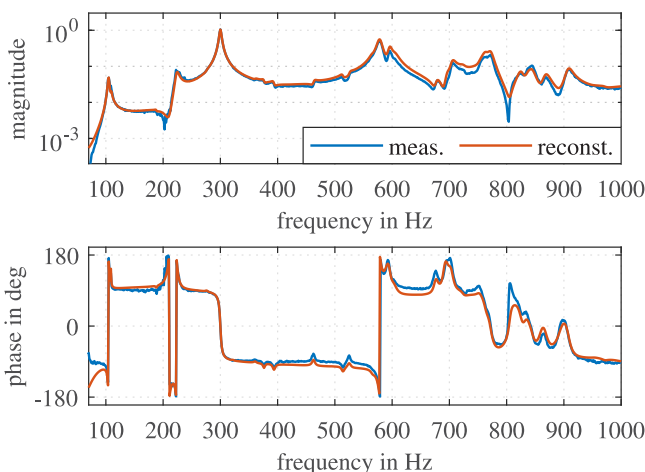


FIG. 9. (Color online) The magnitude (top) and phase (bottom) of the mobility excited on the soundboard and measured below the bridge on the soundboard.

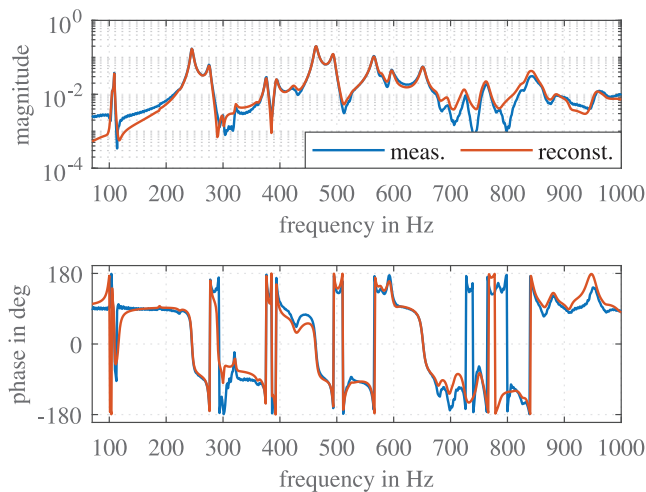


FIG. 10. (Color online) The magnitude (top) and phase (bottom) of the mobility excited on the back and measured on the upper middle part of the back.

mobility below the bridge has only one clear superelevation at 300 Hz and two visible expunctions, one at 200 Hz and one at 800 Hz. Apart from that, the mobility yields rather constant values, arguing for an approximately constant amplification throughout the frequency range.

Last but not least, the identified modal damping ratios ζ_r illustrated in Fig. 11 shall be evaluated. In the frequency range up to 1000 Hz, the values for ζ_r support the claim of a constant damping ratio as they lie constantly between 0.5% and 1%. Only four modal damping ratios lie significantly above that between 1.2% and 1.5%. These particular modes comprise both (0,0)-modes and it is, hence, reasoned that these higher damping ratios might come because of sound radiation rather than material damping.

To sum up, the experimental modal analysis not only reveals valuable information about the guitar, like the constant amplification and constant damping ratio over the frequency range, but is also able to act in the form of eigenfrequencies and mode shapes as a very reliable reference solution to compare the numerical model to.

IV. COMPARISON OF SIMULATION AND EXPERIMENT

So far, a detailed FE model that can meaningfully predict the acoustic structural coupling in the guitar body has

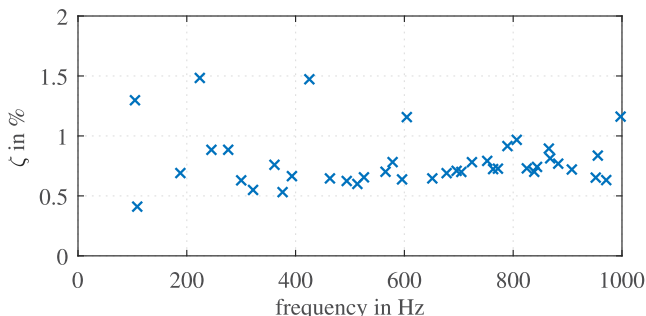


FIG. 11. (Color online) The identified modal damping ratios ζ_r .

been proposed. Additionally, modal parameters of the guitar under investigation have been identified via experimental modal analysis with a high level of reliability. In the following, the numerical model results are compared to the experimental results, and the numerical model is enhanced by identifying the material parameters of the specific guitar.

A. Results with initial material parameters

To validate the FE model, the experimentally identified modal parameters are compared to those calculated with the FE model. The modal assurance criterion (MAC) is often used to indicate the similarity of a mode pair consisting of an experimentally identified mode i and a numerically calculated mode j . The MAC values are calculated as

$$MAC_{ij} = \frac{|\psi_i^H \varphi_j|^2}{\psi_i^H \psi_i \varphi_j^H \varphi_j}, \quad (10)$$

where ψ_i is the mode shape of the measured, experimental mode i and φ_j is the mode shape of the computed, numerical mode j . The MAC values always lie between zero, meaning complete orthogonality of modes, and one, meaning exact conformity of the compared modes (Allemang and Brown, 2006). In most cases, the experimental mode shape vectors are evaluated at far fewer positions than the numerically calculated vectors due to the very fine FE mesh. Therefore, to make the evaluation of the MAC possible, the numerical mode shape vectors φ_j are evaluated only at the closest FE nodes to the points measured with the LDV on the guitar.

In Fig. 12, the MAC matrix comparing the first 15 experimental modes with the first 15 numerical modes is displayed in the shape of a heatmap. Several mode pairs (experimental mode, numerical mode) can be correlated

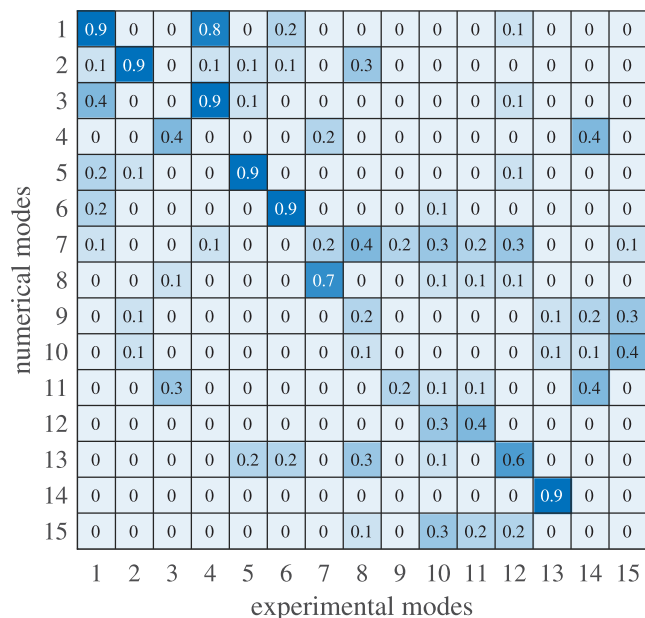


FIG. 12. (Color online) The MAC matrix to numerically compare experimentally identified and simulated modes (values rounded to one significant digit).

without any doubt, like the mode pairs (1,1), (2,2), (5,5), and (6,6), yielding unambiguous MAC values above 0.9. Still obvious are the pairs (4,3) and (7,8), which yield MAC values above 0.7. The modes above the eighth mode, alas, cannot be reproduced by the current configuration of the model. Due to the detailed modeling process, the most significant model error is expected to be induced by the material parameters taken from the literature, which are known to yield a relatively high uncertainty (Kretschmann, 2010). The influence on density and stiffness caused by the varnish further increases this uncertainty (Lämmlein *et al.*, 2020). Therefore, it is accounted to be reasonable to identify the material parameters of the guitar in a range of $\pm 30\%$ around the literature values.

B. Identification of material parameters

Identifying the material parameters for the guitar model is not regarded as a straightforward problem as the parameter space comprises 54 independent material parameters. This number results first from four materials with volumetric elements each having ten independent material parameters [mahogany (neck, head), spruce (bracing), ebony (fretboard), and rosewood (bridge)]. Second, the two regions discretized with shell elements each account for seven additional material parameters [cedar (soundboard), mahogany (back, sides)]. Furthermore, the literature values do not seem to be a good starting point for a gradient-based procedure as too many modes differ significantly between the experiment and numerical models. Thus, instead of a gradient-based numerical optimization, the material parameters are identified via a structured sampling of the parameter space using a Sobol sequence. Sobol sequences are quasi-random sequences to form successively finer uniformly distributed points in an s -dimensional unit hypercube (Sobol *et al.*, 2011). They yield the advantage to cover the space well already with a limited number of parameter sets.

A further necessary step is to reduce the number of independent parameters. This is achieved by eliminating all Poisson ratios from the parameter vector because of their relatively small influence on the modal parameters and by assuming the stiffness parameters of each material to vary uniformly such that

$$\begin{aligned} \frac{E_{L_m}(\mathbf{p})}{E_{L_m}^0} &= \frac{E_{T_m}(\mathbf{p})}{E_{T_m}^0} = \frac{E_{R_m}(\mathbf{p})}{E_{R_m}^0} \\ &= \frac{G_{LT_m}(\mathbf{p})}{G_{LT_m}^0} = \frac{G_{LR_m}(\mathbf{p})}{G_{LR_m}^0} = \frac{G_{TR_m}(\mathbf{p})}{G_{TR_m}^0} \end{aligned} \quad (11)$$

holds for each material m . The superscript “0” denotes the initial parameters. Hence, for each material m , only two independent parameters

$$\mathbf{p}_m = [\mathbf{p}_m^\rho, \mathbf{p}_m^{\text{stiff}}] \quad (12)$$

remain, where \mathbf{p}_m^ρ is the change of density and $\mathbf{p}_m^{\text{stiff}}$ is the change of the Young’s moduli and shear moduli. This results in a parameter space containing 12 independent

TABLE II. Identified material parameters for the different parts of the guitar body.

Part	Material	ρ (kg/m ³)	E_L (GPa)	E_T (GPa)(GPa)	E_R (GPa)	G_{LT} (GPa)	G_{LR} (GPa)	G_{TR} (GPa)
Neck, head	Mahogany	463	7.66	0.382	0.844	0.451	0.672	0.160
Back, sides	Mahogany	656	12.4	0.619	—	0.730	1.09	0.260
Soundboard	Cedar	328	9.85	0.542	—	0.846	0.857	0.049
Bracing	Spruce	387	15.3	0.657	1.190	0.933	0.978	0.046
Fretboard	Ebony	1310	14.7	0.734	1.470	1.030	1.320	0.294
Bridge	Rosewood	609	15.8	0.820	1.64	1.17	1.52	0.351

parameters for the sampling process. To evaluate the results for the different parameter sets \mathbf{p} , the objective function,

$$\varepsilon = \sum_{r=1}^R \left[\left(\frac{\omega_r^{\text{Exp}} - \omega_r(\mathbf{p})}{\omega_r^{\text{Exp}}} \right)^2 + \left(\frac{1 - \sqrt{\text{MAC}_{rr}(\mathbf{p})}}{\sqrt{\text{MAC}_{rr}(\mathbf{p})}} \right)^2 \right], \tag{13}$$

is proposed to rate the eigenfrequency and mode shape deviation for each mode r . The resulting optimization problem reads

$$\mathbf{p}^* = \arg \min_{\mathbf{p} \in P} \varepsilon(\mathbf{p})$$

$$\text{with } P = \{ \mathbf{p} \in \mathbb{R}^{12} \mid 0.7\mathbf{p}_0 \leq \mathbf{p} \leq 1.3\mathbf{p}_0 \}, \tag{14}$$

where the initial parameter values are denoted as \mathbf{p}_0 .

A total of 2000 samples with parameter sets from a Sobol sequence were calculated and in the following, the best result corresponding to Eq. (14) is investigated. It is worth mentioning that the presented parameter set is not an optimal parameter set but the most reasonable parameter set out of 2000 candidates. The resulting parameters are included in Table II, and the relative deviation to the initial values is laid out in Fig. 13. Most of the parameters changed significantly compared to the initial values, and clear tendencies can be drawn from Fig. 13. The soundboard, bridge, and bracing became lighter and stiffer. The opposite is the case for the neck and fretboard, which became heavier and less stiff. Furthermore, the weight and stiffness of the back

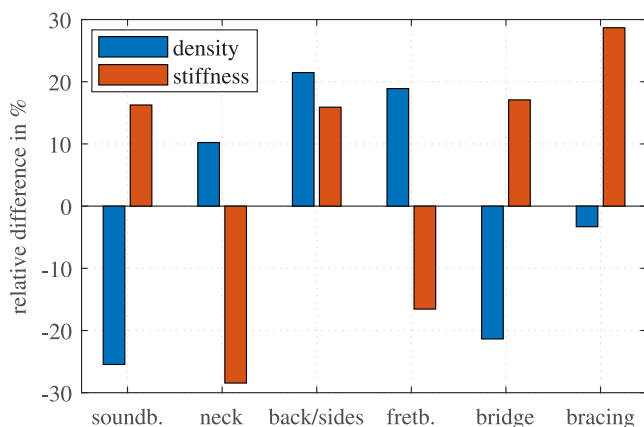


FIG. 13. (Color online) Relative difference of updated parameters (see Table II) to initial ones (see Sec. II B).

and sides increased. The total mass of the model with the updated parameters calculates to $m_{\text{uFE}} = 1470$ g, which is 40 g heavier than the actual guitar. Thus, all of the parameters are considered to lie in a reasonable range, and the total weight of the guitar model is even 10 g closer to the actual value than it was initially; see Sec. II B. It is worth mentioning that multiple local minima exist for the optimization problem, and the solution is close to one of those local minima. With the presented method, it is, hence, not guaranteed that the global minimum is found. Even if the global minimum was found, the results still might not necessarily reflect the actual material properties of the instrument under investigation as other modeling assumptions might lead to a different global minimum.

The numerical results for the modal parameters obtained with the updated material parameters are remarkable, especially for the mode shapes. The first 14 mode shapes occur in the correct order, and all yield MAC values above 0.7 as depicted in Fig. 14, indicating very similar mode shapes in the simulation and experiment. This result is corroborated with Fig. 15 in which three experimentally identified modes and three associated numerically calculated modes are displayed. Even the 13th modes look practically

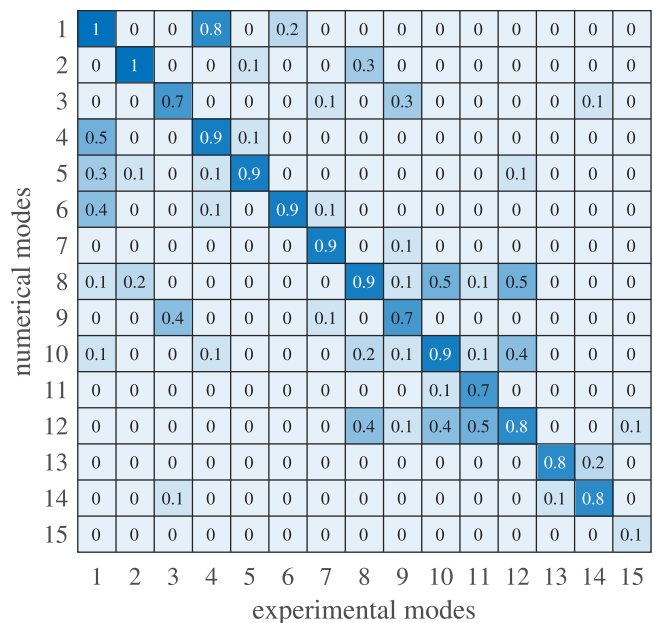


FIG. 14. (Color online) The MAC matrix to numerically compare the experimentally identified and simulated modes with updated parameters (values rounded to one significant digit).

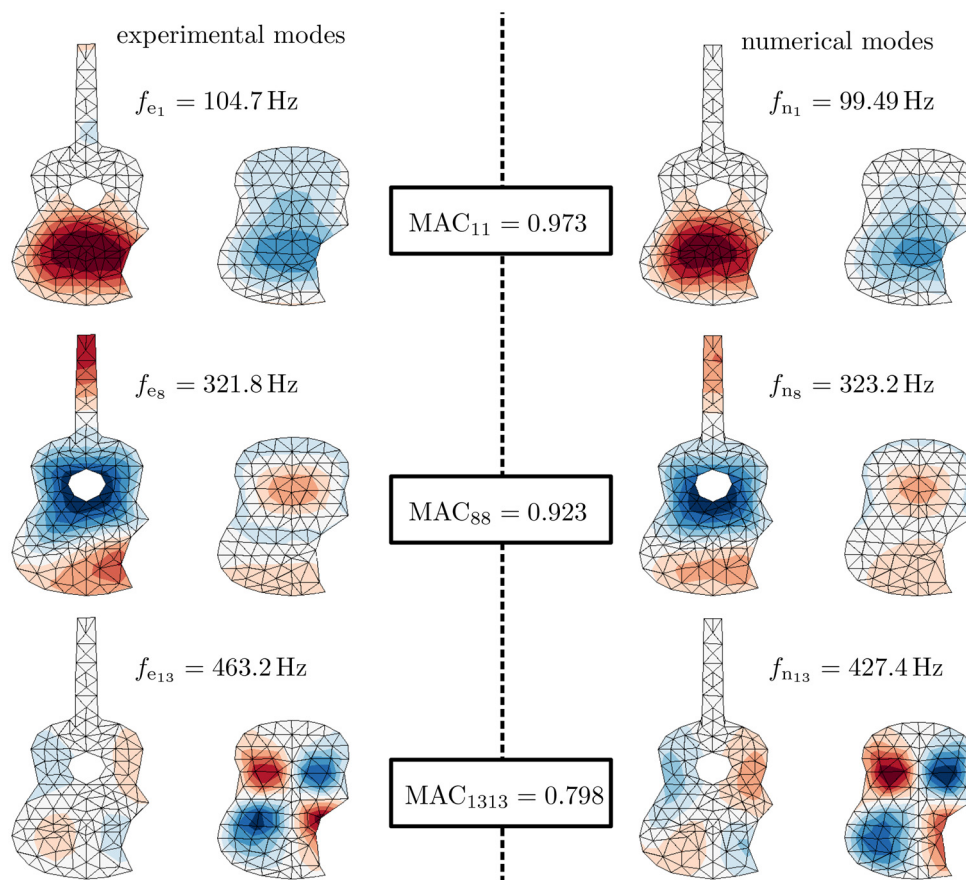


FIG. 15. (Color online) The confrontation of corresponding experimentally identified (left) and numerically calculated (right) eigenmodes.

similar, still yielding a MAC value of 0.8. The visible mesh displays the points measured with the LDV. Both the measurements and FE model results are evaluated at these points or at the nearest node to that in the FE model. The missing corners in the representations are caused by the shadow of the shaker that excited the guitar in the experiment.

Moreover, the eigenfrequencies of the numerical model are very close to the experimentally identified eigenfrequencies as can be seen in Fig. 16. Therefore, the correspondence is very satisfying not only for the mode shapes but also for the eigenfrequencies. However, especially the higher frequencies seem to be systematically lower in the numerical

model. This might correspond to the overall higher mass of the numerical model compared to the actual guitar.

Considering the presented results, the modeling procedure and parameter identification are deemed highly successful. It is possible to identify the material parameters in a realistic range such that the numerical model reproduces the experimentally identified modal parameters in a frequency range up to 500 Hz very well. The deviation, which still occurs, might be explained by the slightly overestimated mass of the model and the reduced parameter vector for the parameter identification procedure.

V. CONCLUSION

A comprehensive reverse-engineering procedure to create a detailed FE model of an existing classical guitar is proposed. The most influential factors of such a model are identified and methods to include them are suggested. First, the detailed reconstruction of the geometry is possible with CT scans of the instrument. Second, the fluid-structure interaction between the guitar body and enclosed air is included in the modeling procedure. Additionally, the orthotropic material properties taken from the literature are enhanced to account for the weight increase due to the varnish. To validate the model and, hence, the reverse-engineering procedure, a modal analysis technique using the CMIF is used, which has proven to deliver reliable results to act as a

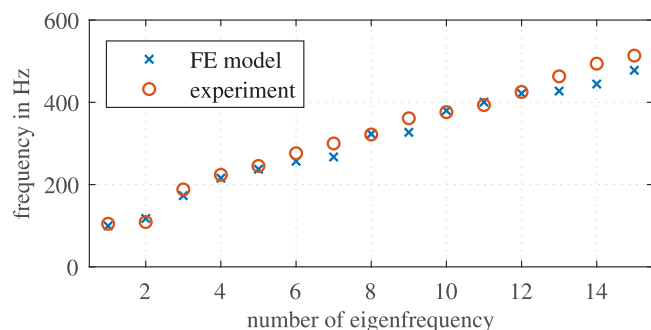


FIG. 16. (Color online) The eigenfrequencies of the corresponding modes calculated numerically and identified experimentally.

reference solution. Using the experimental results, it is shown that it is possible to identify the material parameters for the whole instrument in a realistic range such that the model reproduces the modal parameters of the actual instrument in a frequency range up to 500 Hz. However, the identified material parameters cannot be interpreted as the actual material properties of the instrument under investigation as the parameters only represent one of multiple possible parameter sets.

All in all, the proposed procedure is well suited to create high-fidelity FE models of existing instruments. The presented model will not only be of use to simulate the influence of the modifications on the instrument but as a result of its high fidelity, it will also be used to develop further parameter identification strategies or gain further insight into the physical behavior of classical guitars in general.

ACKNOWLEDGMENTS

The authors would like to thank the Department of Diagnostic and Interventional Radiology of the *Klinikum Stuttgart* and its director Professor Dr. Götz Martin Richter for providing the CT scans and especially Stephanie Hollenhorst for conducting these CT scans after her regular working hours. Parts of this research were supported by the German Research Foundation DFG (Project No. 455440338). This support is highly appreciated.

Abaqus. (2014). *Analysis User's Guide* (Simulia, Providence).
 Allemang, R., and Brown, D. (2006). "A complete review of the complex mode indicator function (CMIF) with applications," in *Proceedings of ISMA International Conference on Noise and Vibration Engineering*.
 Bader, R. (2006). *Computational Mechanics of the Classical Guitar* (Springer Science and Business Media, Berlin).
 Bécache, E., Chaigne, A., Derveaux, G., and Joly, P. (2005). "Numerical simulation of a guitar," *Comput. Struct.* **83**(2-3), 107–126.
 Boullosa, R. R. (2002). "Vibration measurements in the classical guitar," *Appl. Acoust.* **63**(3), 311–322.
 Brauchler, A., Ziegler, P., and Eberhard, P. (2020a). "Examination of polarization coupling in a plucked musical instrument string via experiments and simulations," *Acta Acust.* **4**(3), 9.
 Brauchler, A., Ziegler, P., and Eberhard, P. (2020b). "Numerical models for classical guitars with updated parameters from experimental data," in *Proceedings of Forum Acusticum 2020*, Lyon.
 Buzug, T. (2011). *Computed Tomography* (Springer, Berlin), pp. 311–342.
 Caldersmith, G. (1978). "Guitar as a reflex enclosure," *J. Acoust. Soc. Am.* **63**(5), 1566–1575.
 Chomette, B., and Le Carrou, J.-L. (2015). "Operational modal analysis applied to the concert harp," *Mech. Syst. Signal Process.* **56-57**, 81–91.
 Christensen, O. (1982). "Quantitative models for low frequency guitar function," *J. Guitar Acoust.* **6**, 10–25.
 Derveaux, G., Chaigne, A., Joly, P., and Bécache, E. (2003). "Time-domain simulation of a guitar: Model and method," *J. Acoust. Soc. Am.* **114**(6), 3368–3383.
 Ducceschi, M., and Bilbao, S. (2016). "Linear stiff string vibrations in musical acoustics: Assessment and comparison of models," *J. Acoust. Soc. Am.* **140**(4), 2445–2454.
 Elejabarrieta, M., Ezcurra, A., and Santamaria, C. (2000). "Evolution of the vibrational behavior of a guitar soundboard along successive construction phases by means of the modal analysis technique," *J. Acoust. Soc. Am.* **108**(1), 369–378.
 Ewins, D. (2000). *Modal Testing, Theory, Practice, and Application*, 2nd ed. (Research Studies, Baldock).

Ezcurra, A., Elejabarrieta, M., and Santamaria, C. (2005). "Fluid–structure coupling in the guitar box: Numerical and experimental comparative study," *Appl. Acoust.* **66**(4), 411–425.
 Fletcher, N., and Rossing, T. (1991). *The Physics of Musical Instruments* (Springer Science and Business Media, New York).
 French, M. (2007). "Structural modification of stringed instruments," *Mech. Syst. Signal Process.* **21**(1), 98–107.
 Fritz, C., Curtin, J., Poitevineau, J., Morrel-Samuels, P., and Tao, F. (2012). "Player preferences among new and old violins," *Proc. Nat. Acad. Sci. U.S.A.* **109**(3), 760–763.
 Gore, T. (2011). "Wood for guitars," *Proc. Mtgs. Acoust.* **12**, 035001.
 Hiller, L., and Ruiz, P. (1971). "Synthesizing musical sounds by solving the wave equation for vibrating objects: Part 1," *J. Audio Eng. Soc.* **19**(6), 462–470.
 Issanchou, C., Le Carrou, J., Touzé, C., Fabre, B., and Doaré, O. (2018). "String/frets contacts in the electric bass sound: Simulations and experiments," *Appl. Acoust.* **129**, 217–228.
 Konopka, D., Gebhardt, C., and Kaliske, M. (2017). "Numerical modelling of wooden structures," *J. Cult. Heritage* **27**, S93–S102.
 Kretschmann, D. (2010). "Mechanical properties of wood," in *Wood Handbook: Wood as an Engineering Material* (Forest Products Laboratory, Madison), available at https://www.fpl.fs.fed.us/documnts/fplgtr/fpl_gtr190.pdf (Last viewed 14 June 2021).
 Lämmlein, S., Van Damme, B., Mannes, D., Schwarze, F., and Burgert, I. (2020). "Violin varnish induced changes in the vibro-mechanical properties of spruce and maple wood," *Holzforschung* **1**, 765–776.
 Popp, J. (2012). "Four mass coupled oscillator guitar model," *J. Acoust. Soc. Am.* **131**(1), 829–836.
 Pyrkosz, M. A. (2013). "Reverse engineering the structural and acoustic behavior of a Stradivari violin," Ph.D. thesis, Michigan Technological University, Houghton, Michigan.
 Richardson, B., and Roberts, G. (1983). "The adjustment of mode frequencies in guitars: A study by means of holographic interferometry and finite element analysis," in *Proceedings of the Stockholm Music Acoustics Conference*, Stockholm, Vol. 83, pp. 285–302.
 Saitis, C., Giordano, B., Fritz, C., and Scavone, G. (2012). "Perceptual evaluation of violins: A quantitative analysis of preference judgments by experienced players," *J. Acoust. Soc. Am.* **132**(6), 4002–4012.
 Šali, S., and Kopač, J. (2000). "Measuring the quality of guitar tone," *Exp. Mech.* **40**(3), 242–247.
 Sigrist, J.-F. (2015). *Fluid-Structure Interaction: An Introduction to Finite Element Coupling* (Wiley, Hoboken, NJ).
 Sobol, I., Asotsky, D., Kreinin, A., and Kucherenko, S. (2011). "Construction and comparison of high-dimensional sobol generators," *Wilmott* **2011**(56), 64–79.
 Stanciu, M. D., Vlase, S., and Marin, M. (2019). "Vibration analysis of a guitar considered as a symmetrical mechanical system," *Symmetry* **11**(6), 727.
 Tahvanainen, H., Matsuda, H., and Shinoda, R. (2019). "Numerical simulation of the acoustic guitar in virtual prototyping," in *Proceedings of ISMA 2019*, Detmold.
 Torres, J., and Boullosa, R. (2009). "Influence of the bridge on the vibrations of the top plate of a classical guitar," *Appl. Acoust.* **70**(11-12), 1371–1377.
 Torres, J. A., Soto, C. A., and Torres-Torres, D. (2020). "Exploring design variations of the titian Stradivari violin using a finite element model," *J. Acoust. Soc. Am.* **148**(3), 1496–1506.
 Torres, J. A., and Torres-Martínez, R. (2015). "Evaluation of guitars and violins made using alternative woods through mobility measurements," *Arch. Acoust.* **40**(3), 351–358.
 Välimäki, V., Pakarinen, J., Erkut, C., and Karjalainen, M. (2006). "Discrete-time modelling of musical instruments," *Rep. Prog. Phys.* **69**(1), 1–78.
 Viala, R., Placet, V., and Cogan, S. (2018). "Identification of the anisotropic elastic and damping properties of complex shape composite parts using an inverse method based on finite element model updating and 3D velocity fields measurements (FEMU-3DVF): Application to bio-based composite violin soundboards," *Compos. Part A: Appl. Sci. Manuf.* **106**, 91–103.
 Viala, R., Placet, V., Le Conte, S., Vaiedelich, S., and Cogan, S. (2020). "Model-based decision support methods applied to the conservation of

musical instruments: Application to an antique cello,” in *Model Validation and Uncertainty Quantification*, 3rd ed. (Springer, Cham, Switzerland), pp. 223–227.

Wegst, U. G. K. (2006). “Wood for sound,” *Am. J. Botany* **93**(10), 1439–1448.

Woodhouse, J. (2004a). “On the synthesis of guitar plucks,” *Acta Acust. Acust.* **90**(5), 928–944.

Woodhouse, J. (2004b). “Plucked guitar transients: Comparison of measurements and synthesis,” *Acta Acust. Acust.* **90**(5), 945–965.